Endwall Film Cooling Effects on Secondary Flows in a Contoured Endwall Nozzle Vane

Giovanna Barigozzi
e-mail: giovanna.barigozzi@unibg.it

Giuseppe Franchini
e-mail: giuseppe.franchini@unibg.it

Antonio Perdichizzi
e-mail: antonio.perdichizzi@unibg.it

Marco Quattrore

Dipartimento di Ingegneria Industriale,
Università degli Studi di Bergamo,
Viale Marconi,
24044 Dalmine (BG), Italy

The present paper investigates the effects of endwall injection of cooling flow on the aerodynamic performance of a nozzle vane cascade with endwall contouring. Tests have been performed on a seven vane cascade with a geometry typical of a real gas turbine nozzle vane. The cooling scheme consists of four rows of cylindrical holes. Tests have been carried out at low speed ($Ma_{2is}=0.2$) with a low inlet turbulence intensity level (1.0%) and with a coolant to mainstream mass flow ratio varied in the range from 0% (solid endwall) to 2.5%. Energy loss coefficient, secondary vorticity, and outlet angle distributions were computed from five-hole probe measured data. Contoured endwall results, with and without film cooling, were compared with planar endwall data. Endwall contouring was responsible for a significant overall loss decrease, as a result of the reduction in both profile and planar side secondary flows losses; a loss increase on the contoured side was instead observed. Like as for the planar endwall, even for the contoured endwall, coolant injection modifies secondary flows, reducing their intensity, but the relevance of the changes is reduced. Nevertheless, for all the tested injection conditions, secondary losses on the contoured side are always higher than in the planar case, while contoured cascade overall losses are lower. A unique minimum overall loss injection condition was found for both tested geometries, which corresponds to an injected mass flow rate of about 1.0%. [DOI: 10.1115/1.3192147]

1 Introduction

The increase in gas turbine performance requires the enhancement of thermal protection all over the turbine surfaces, including the endwall region. In fact, the increase in turbine inlet temperature and the improvement of combustor design combine to give higher and flatter temperature distributions in front of the first nozzle vane. To reduce the cost of production, in modern gas turbines, the first stage is highly loaded and the vane is characterized by a high pitch-to-chord ratio. The cooling scheme is a major contributor to the complexity of the design/manufacturing. Furthermore low aspect ratios are usually adopted. Both these features act to enhance the secondary flow intensity, so that secondary losses become comparable or even larger than the profile losses.

In modern gas turbines, the transition from the combustion chamber to the turbine needs a flow passage area reduction; this can be accomplished by profiling the casing in the first vane. Dejc et al. [1] reported on the efficiency improvement due to endwall contouring in rotating rigs. The major acceleration due to the greater channel convergence reduced the profile losses and inhibited the secondary flows development. Boletis [2], using a detailed flow field analysis in an annular cascade with outer diameter endwall contouring, found that the pitchwise pressure gradient in the front of the cascade was significantly reduced, thus causing lower secondary losses. Moustapha and Williamson [3], after testing two different endwall shapes with the same height contraction, substantially confirmed Boletis results. Dossena et al. [4] reported a combined experimental and numerical investigation performed on the same vane and contouring geometry object of the present investigation, but tested at a higher Mach number of 0.6. The comparison between the flat and contoured endwall results gave evidence that the streamwise channel contraction produces a lower loss level, affecting both profile and secondary losses.

The flow pattern close to the solid surfaces determines the heat transfer coefficient distribution and, when film cooling is adopted, it governs the interaction between the injected cooling air and the hot mainstream. Sieverding and Wilputte [5], testing a straight nozzle cascade, showed a significant influence of endwall cooling air injection upon the losses and exit air angle distribution. Since then, many authors have enlightened the mutual interaction between endwall coolant jets and secondary flows (e.g., see Refs. [6,7]). In particular, Friedrichs et al. [8,9] showed that the endwall coolant injection strongly alters the secondary flow structure, with the lift-off line of the horseshoe vortex moving closer to the leading edge when coolant injection is present. When the coolant is injected at large mass flow rates, it re-energizes the boundary layer, thus weakening the secondary flows.

More recently, Nicklas and co-worker [10,11] investigated the aerothermal behavior of a transonic cascade with endwall film cooling. A strong interaction between the coolant and the main flow was detected. Again, coolant injection strengthens the endwall boundary layer, thus reducing the endwall crossflow. A similar investigation, but on a different endwall cooling scheme, was also performed by Knost and Thole [12]. They found that coolant behavior is strongly dependent on local blowing conditions for the cooling holes, and especially on the momentum flux ratio. The leading edge region and pressure side were found to be the most difficult regions to be efficiently cooled. Barigozzi et al. [13,14] compared a cylindrical cooling scheme with respect to a fan-shaped planar endwall cooling configuration; in both cases, they found that coolant injection strongly alters the secondary flow behavior. A minimum loss was found for the cylindrical cooling scheme for a mass flow rate of about 1%, which corresponds to an inlet loss free blowing ratio of 2.0. The introduction of a conical expanded exit increased the coolant protection capabilities at high injection rates. This was obtained by paying a "thermodynamic" loss increase; nevertheless, the passage vortex activity was significantly reduced.

Contributed by the International Gas Turbine Institute of ASME for publication in the JOURNAL OF TURBOMACHINERY. Manuscript received June 30, 2008; final manuscript received February 10, 2009; published online April 27, 2010. Review conducted by David Wisler. Paper presented at the ASME Turbo Expo 2008: Land, Sea and Air (GT2008), Berlin, Germany, June 9–13, 2008.

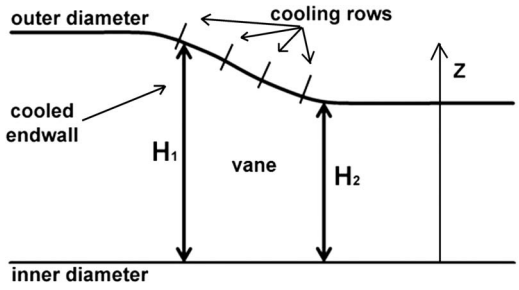

Fig. 1 Meridional profile

Most of reported researches are related to film cooling applied to flat endwalls. Much few investigations documenting the combining effects of endwall contouring and cooling are available; among them, the experimental investigations performed at the University of Minnesota [15,16] on both slot and discrete holes bleed injection over a contoured endwall nozzle guide vane cascade. The slot results showed a substantially unchanged flow field at low bleed flow rates. Increasing the injected bleed flow, the secondary flow structure near the contoured endwall was instead progressively suppressed. No information on the secondary flow structure with discrete hole configurations was given. Beneficial effects on the aerodynamic performance of an asymmetric endwall cascade due to discrete holes endwall film cooling was also documented by Gustafson et al. [17].

The present paper deals with the effects of endwall film cooling and overall mass flow ratio on the aerodynamic performance of a nozzle vane cascade with outer diameter profiling. The same cascade was already extensively tested at a low Mach number of 0.2 on a straight configuration with and without endwall film cooling [13,14,18], while Dossena et al. [4] reported data obtained at a higher Mach number of 0.6 with endwall contouring but without film cooling. In the present paper, 3D flow field configurations with and without coolant injection on contoured endwall will be compared with flat endwall results. Secondary flow modification due to coolant injection at different blowing conditions will be analyzed and discussed in details.

2 Experimental Details

2.1 Geometry and Test Conditions. Tests were performed in the subsonic wind tunnel for linear cascades at the Turbomachinery and Energy Conversion Systems Laboratory at Bergamo University. The wind tunnel has been modified in order to make the meridional channel passage area reduction depicted in Fig. 1. The endwall profile is characterized by a streamwise span contraction $H_2/H_1=0.70$. A modular design of the contoured endwall, manufactured by using a rapid prototyping machine, allows to easily substitute the solid endwall of the two central passages with a cooled one. Figure 2 shows a picture of the new contoured endwall wind tunnel.

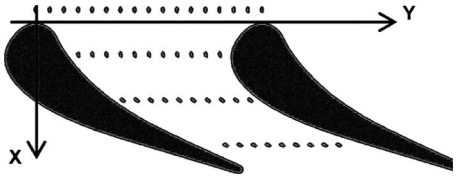

Fig. 3 Cascade and endwall cooling geometry—CONF1

Details of the cascade geometry and the secondary air supply system are given in Ref. [13]. The facility consists of a seven-blade cascade, whose geometry is typical of a first stage high pressure nozzle vane. Figure 3 shows the tested vane together with the cooled endwall geometry. In order to obtain information directly comparable with previous results, the contoured cascade was not restaggered. This will imply a different tangential flow angle at midspan with respect to the planar cascade. As high speed results have shown only a difference of about 1 deg at the cascade exit, the comparison between the flat and contoured results can be accepted. Moreover, the focus of this investigation is to assess the effects of coolant injection on the loss distributions downstream of the cascade, rather than to investigate the effect of endwall contouring, which has been already well faced by previous studies.

Only the contoured endwall is cooled, with cooling assured by the presence of four rows of cylindrical holes with 1.5 mm diameter (corresponding to a cascade pitch-to-hole diameter of about 76.67) connected to a single plenum. A major difference, with respect to previous analysis, is the presence of two cooled vane passages instead of only one. Hole locations and geometrical characteristics are summarized in Table 1 and Fig. 4; the configuration is the same as previously adopted in the flat endwall study, where it was named CONF1. In particular, row A is located upstream of the leading edge plane. The following three rows are evenly positioned inside the vane channel, with the last one located at 82% c_{ax} downstream of the leading edge plane. Row C is located where the horseshoe vortex separation line (in the flat endwall) impacts

Table 1 Cooling system geometrical characteristics

	Row			
	A	B	C	D
X/c_{ax}	−0.09	0.21	0.51	0.81
N	17	11	10	9
P/D		4.8		
L/D		10.7		
α		30 deg		

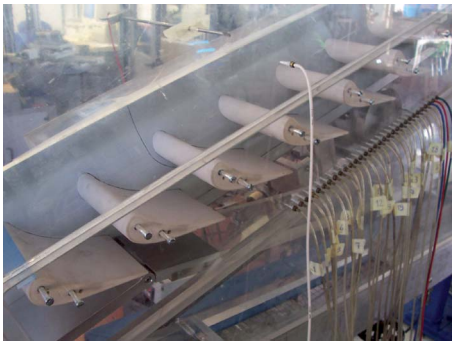

Fig. 2 Wind tunnel test section

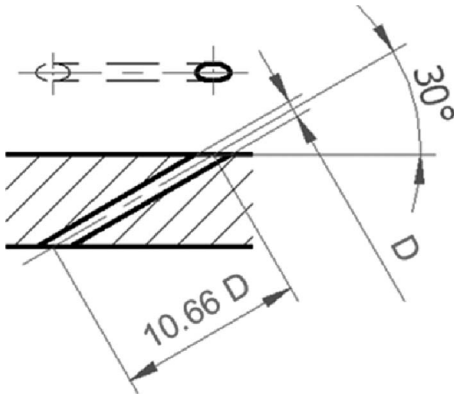

Fig. 4 Detail of CONF1 hole geometry

Table 2 Contoured cascade geometry and operating conditions

$s/c=0.86$	$H_1/c=1.04$
$c=133.7$ mm	$H_2/H_1=0.7$
$\beta_1=0$ deg	$\beta_2'=79$ deg
$Ma_1=0.047$	$Ma_{2is}=0.2$
$Re_{2is}=0.66\times10^6$	$Tu_1=1\%$

on the suction side surface [13]. Hole injection angle has been set to 30 deg with respect to the endwall surface. In the blade to blade plane, each row has a compound angle equal to the mean flow angle at midspan.

The cascade geometry and the operating conditions are summarized in Table 2. Tests were performed at low isentropic Mach number ($Ma_{2is}=0.2$), and low inlet turbulence intensity, namely, 1%. Figure 5 compares the actual planar low speed profile isentropic Mach number distribution and the ones measured by Dossena et al. [4] at a higher Ma_{2is} of 0.6 on both planar and contoured cascades at midspan. To make the comparison easiest, data are normalized with the outlet isentropic Mach number. Figure 5 clearly shows that, for the planar configuration, the reduced Mach number slightly anticipates recompression; it starts at $X/c=0.2$ against 0.3 at $Ma_{2is}=0.6$. As no compressibility effects take place and no significant diffusion modification was noticed, a similar and relevant profile Mach number distribution variation due to endwall contouring can be expected at low Mach number. Following Dossena et al. [4], with a contoured endwall, a lower diffusion rate over the whole rear suction surface is likely to take place, as well as a reduced vane front loading, resulting in a reduced profile loss.

Air at ambient temperature was blown as cooling flow. To identify the testing conditions both the overall mass flow ratio *MFR* and the inlet loss free blowing ratio M_1 were determined. The injected mass flow was measured by an orifice device. M_1 values were instead computed using the cascade inlet total and static pressures and the coolant total pressure.

Tests were carried out for *MFR* ranging between 0.0% and 2.5%, which corresponds to M_1 values in the range 0.0–6.0. Figure 6 shows the linear dependency of the overall mass flow ratio *MFR* on the inlet blowing ratio M_1. Data of present analysis are compared with planar cascade data [13,14]. The different pressure distribution on the endwall surface (see Fig. 6) is responsible for the reduced M_1 values of the contoured cascade at constant *MFR*.

The inlet boundary layer was characterized by traversing a flattened pitot tube 80% c_{ax} upstream of the leading edge. The boundary layer profile and integral parameters are reported in Fig. 7 and Table 3, respectively. The new design of the inlet section is responsible for the inlet boundary layer modification. From the boundary layer profile an inlet loss of 0.4% and 0.14% for the planar and profiled cases, respectively, were estimated. A small influence of the boundary layer thickness and inlet turbulence intensity level was observed by the authors testing the planar cascade [18]. Even if some local differences were observed, overall and secondary losses were not affected by these parameters.

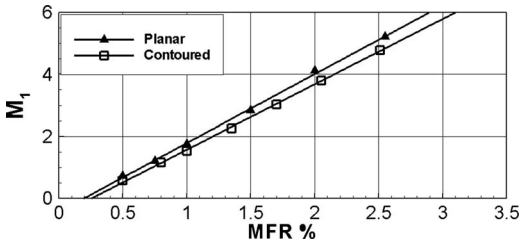

Fig. 6 M_1 versus *MFR*

2.2 Measurement Techniques. Aerodynamic measurements were performed downstream of the trailing edge plane by using a five-hole miniaturized aerodynamic pressure probe (1.6 mm head, advanced 50 mm to the stem). Uncertainties have been estimated to be ±0.15% of dynamic pressure. A fully automated computer controlled data acquisition and probe traversing system has been used. Testing conditions were controlled through a continuous monitoring of the global coolant to mainstream mass flow rate.

The measurement plane is located 50% of the axial chord downstream of the trailing edge ($X/c_{ax}=150\%$) and it covers the two cooled blade passages. The measurement grid consists of 30 points per pitch in tangential direction times 27 points along the blade height. The grid spacing was reduced approaching the endwall surfaces; the first measurement point was 1.65 mm far from the wall. The probe head positioning along the measurement grid was achieved with a fully three-dimensional traversing system.

The coolant flow total pressure and temperature are measured by six pressure taps and six thermocouples located at different axial and tangential positions on the plenum back side wall. As a maximum standard deviation in the six acquired signals of about ±1.5% took place, a uniform plenum total pressure distribution was assumed. The latter was computed by averaging the signals coming from the six available pressure taps.

To measure the contoured endwall pressure distribution, 47 pressure taps were manufactured all over its surface. The pressure

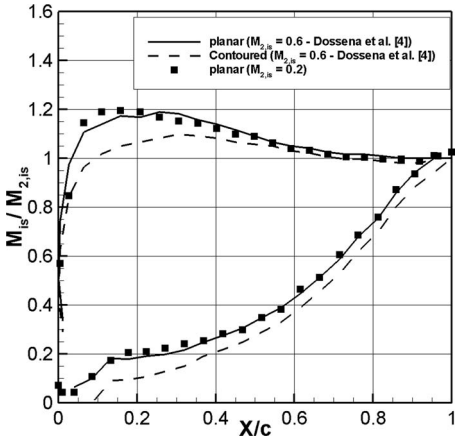

Fig. 5 Isentropic profile Mach number distributions at *Z/H* =0.5

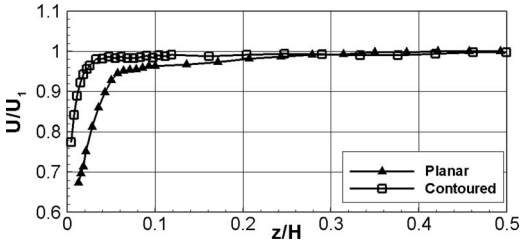

Fig. 7 Inlet boundary layer profile ($X/c_{ax}=-80\%$)

Table 3 Inlet boundary layer integral parameters

	Flat	Contoured
δ (mm)	8.4	4.5
δ^* (mm)	1.36	0.8
H_{12}	1.95	2.14
ζ (%)	0.4	0.14

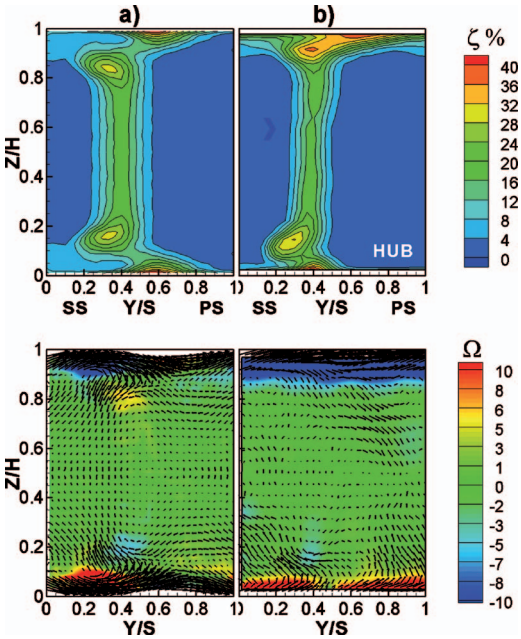

Fig. 8 Solid (*a*) planar and (*b*) contoured cascade secondary kinetic energy loss coefficient; vorticity and velocity vectors ($X/c_{ax}=150\%$)

taps coordinates over the endwall surface correspond to the cooling holes ones, while their axis coincide with the local surface normal direction. All the taps are connected to a 48 channel Scanivalve.

3 Results

Two series of tests were performed in order to analyze the mutual cooling to secondary flow aerodynamic interaction; the first measurement campaign was devoted to compare the secondary flows in the planar and contoured geometry without any platform film cooling. It has to be observed that this comparison should have been performed at constant inlet boundary layer and vane turning. Nevertheless, for the present investigation, it is necessary to define the reference condition and to quantify the modifications endwall contouring produces on the secondary flows and related losses. The second test series investigated the influence of *MFR* on the secondary flow structure downstream of the profiled endwall cascade.

Results will be presented in terms of contour plots of secondary losses and, for the uncooled cases, vorticity computed from the downstream five-hole probe traverses. The streamwise vorticity Ω_s was evaluated from Ω_x and Ω_y. While the experimental results allow a direct estimate of Ω_x, Ω_y was computed in an indirect way by following the procedure suggested by Gregory-Smith et al. [19] based on the Crocco relation. The vorticity values are normalized by using the inlet freestream velocity and the vane chord. Secondary velocity vectors are superimposed to the vorticity distributions.

Local flow field data were then mass averaged over the pitch to obtain both the deviation angle and loss coefficient spanwise distributions. Finally, overall energy loss coefficients have been estimated by mass averaging the flow data all over the vane passage.

It has to be observed that the spanwise coordinate is always normalized with the actual vane span, i.e., H_2. Of course, the outlet blade span for the contoured cascade is 70% smaller than the planar one.

3.1 Solid Endwall. A typical secondary flow configuration characterizes the solid planar endwall cascade (Fig. 8). The flow field is dominated by the presence of a well defined passage vortex, which corresponds to the negative vorticity region (referring to the upper half span) and to the loss core on the suction side of the wake. Due to the large distance from the cascade exit plane ($x/c_{ax}=150\%$), only weak traces of the trailing shed vorticity (positive values) could be found. A significant crossflow, which embeds the corner vortex, can be observed in the endwall region.

The solid contoured endwall results show, as expected, a nonsymmetric loss distribution with an evident wake width reduction. According to Dossena et al. [4], this loss decrease is due to a smaller aerodynamic loading in the front part of the profile and to a reduced diffusion rate over the rear suction surface caused by endwall contouring; thus, a significant profile loss reduction takes place.

At the flat side ($Z/H=0.0$ hub) the loss contours resemble the planar distributions. According to a previous investigation [4], both passage and corner vortex related loss cores slightly move toward the endwall surface, maintaining the same peak values. A general reduction in the secondary vorticity can also be noticed, being this the result of the minor front loading of the profile. Another difference is the position of the loss core related to the corner vortex; it is almost aligned with the wake without the typical pitchwise displacement due to the endwall crossflow. Secondary velocity plot shows a much weaker crossflow, confirming a significant reduction in secondary flows intensity.

On the contoured endwall ($Z/H=1.0$ outer diameter) both loss and vorticity distributions are quite different. The loss core related to the passage vortex looks squeezed at the endwall and joined to the corner vortex. Then a quite strong crossflow extending spanwise can be observed; this crossflow is not related to the normal inlet vorticity, but it is the result of the axial velocity reduction caused by the diffusion occurring at the outer diameter, downstream of the trailing edge. The loss distribution on the contoured side better resembles the one of a developing endwall boundary layer growing under the influence of an adverse pressure gradient. These findings are consistent with results of Dossena et al. [4]. Large negative vorticity values characterize the whole outer diameter endwall region, making the identification of any vortical structure a difficult task. Anyway, from the secondary velocity vector distribution, traces of the corner and passage vortices can be still found very close to the wall.

Starting from the local flow field distributions, data were mass averaged over the pitch to obtain the spanwise distributions of the loss coefficient and deviation angle. The results for the planar and contoured vanes are reported in Fig. 9. It has to be pointed out that the two tested vane models have the same inlet span, but different exit sections; the contoured vane height is 70% smaller than the planar one. So, in comparing the contoured and planar data, one has to consider this difference.

Both planar cascade loss and deviation angle show the typical distribution related to secondary flows. Note that the secondary loss coefficient is defined as the difference between the spanwise and midspan value in order to show any secondary loss difference. Therefore, for a comprehensive evaluation of the overall loss in the two vanes, one has to consider that the profile loss was changed because of different loading conditions.

Comparing the planar and contoured pitch averaged loss distributions (Fig. 9(*a*)), a wider two-dimensional region for the contoured cascade takes place (60% of the span, which corresponds to about 59 mm, against 40% for the planar case, which is 56 mm). Approaching the hub, similar ζ distributions have been found but with lower values for the contouring case, except very close to the surface.

Quite different patterns take place on the outer diameter side; a sharp increase in ζ occurs for the contouring cascade. This behavior is both due to the higher wetted surface and to the adverse pressure gradient that the flow experiences downstream of the cascade exit plane, as documented by Dossena et al. [4].

Figure 9(*b*) presents the pitch averaged deviation angle distributions for the two tested endwall geometries. Note that all data

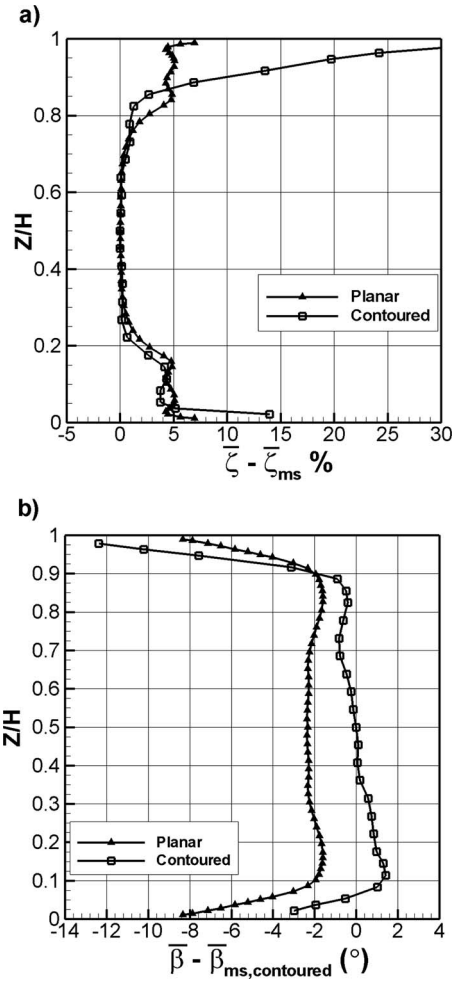

Fig. 9 Spanwise (*a*) primary loss and (*b*) flow angle deviation distribution

are referred to the midspan flow angle of the contoured vane, being this about 2 deg higher than the one in the planar case; this is because the two cascades, i.e., planar and contoured, have been manufactured with the same stagger angle. It can be seen that for the profiled vane an almost linear flow angle distribution takes place over most of the span. This exit angle distribution is surely positive for the design of the following rotor blade, as it reduces the relative flow angle variation from hub to tip.

Mass averaging the flow data also in spanwise direction, thus all over the vane passage, overall energy loss coefficients have been computed as

$$\bar{\bar{\zeta}} = \frac{\bar{\bar{U}}_{2is}^2 - \bar{\bar{U}}_2^2}{\bar{U}_{2is,ms}^2} \tag{1}$$

Table 4 compares the different contributions to loss generation for the two vanes, reporting the profile losses, secondary losses from the flat and contoured endwalls, and overall losses. The secondary loss is obtained by subtracting the pitchwise averaged loss at midspan from the total loss. For the contoured endwall, mass averaging was performed twice: from midspan to the contoured side and from midspan to the flat side. Table 4 shows that profiling the endwall produces a significant reduction in the overall losses: 5.13% against 6.5%. This is not a direct effect of the secondary flow losses on the contoured side, but it is the result of a global improvement of the cascade performance. Secondary losses on the flat side undergo a reduction of 0.56%, resulting from less intense secondary flow effects. On the contoured side, on the contrary,

Table 4 Mass averaged losses

		ζ (%)	
		Flat	Contoured
Overall		6.5	5.13
Profile		4.3	2.81
Secondary Z/H	0–100%	2.2	2.32
	0–50%	2.2	1.64
	50–100%	2.2	2.99

there is a loss increase of 0.79%; this is likely due to the larger wet surface, to the significant diffusion, which takes place downstream of the trailing edge and to the endwall curvature. Therefore, most of the overall loss reduction is related to the lower profile loss, which is the consequence of a lower front loading and a minor diffusion after the throat.

3.2 Local Blowing Ratios. Before discussing the influence of coolant to mainstream mass flow rate on the secondary flows, the reader is reminded that local injection conditions are strongly influenced by the local values of parameters, like blowing and momentum flux ratios. Since all the holes belonging to the two cooled vane passages are fed by a single plenum, such parameters experience large variations in both pitchwise and streamwise directions because of the large variation in static pressure on the endwall surface. Figure 10 reports the isentropic Mach number distribution computed from the inlet cascade total pressure and the static pressure distribution measured by means of the pressure taps distributed all over the contoured endwall surface. The Mach number distribution of the planar cascade is also reported for comparison, even if it was measured at midspan by means of a laser Doppler anemometer.

Figure 10 clearly shows a different Mach number distribution for the two endwall geometries. In particular, the contoured endwall shows lower velocities in the channel front part, as both tests were run at the same outlet isentropic Mach number; this confirms the decreased aerodynamic loading in the front part of the profile, just where the secondary flows are going to develop.

The different endwall pressure distributions give rise to a different coolant mass flow sharing among rows and also among the

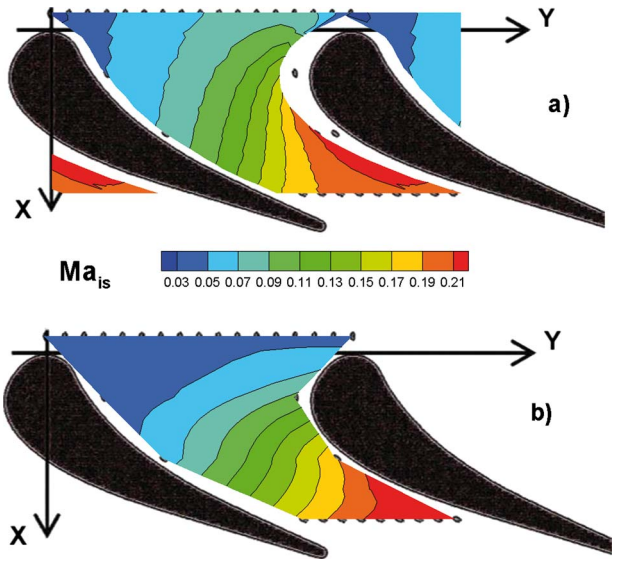

Fig. 10 Local Mach number: (*a*) planar cascade midspan distribution (solid) and (*b*) contoured cascade isentropic endwall distribution

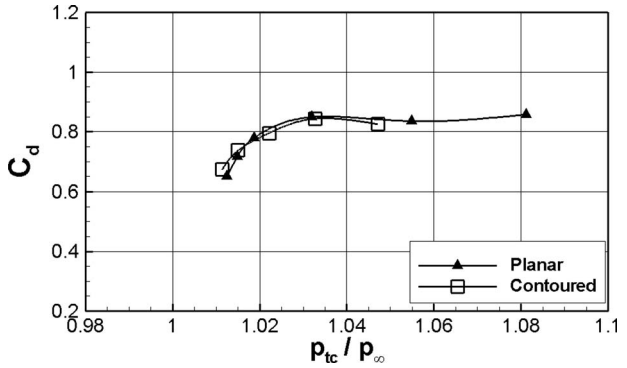

Fig. 11 Discharge coefficients

different holes belonging to each row. To compute the local blowing ratios, the discharge coefficient C_d was measured with all the holes blowing. Figure 11 shows the C_d values versus the pressure ratio between the plenum total pressure and the average static pressure measured at the endwall surface where injection holes are located. Also reported are the planar cascade data; no significant differences between the two distributions can be observed.

Local blowing ratios were then computed to identify the local injection conditions. The exit coolant velocity was evaluated from the ideal hole flow rate and the average discharge coefficient. Figure 12 shows the local *BR* values obtained for the contoured endwall geometry and the tested *MFR*. Also reported for comparison are the corresponding blowing ratio values of the planar case. According to the endwall pressure distribution reported in Fig. 10, for the first row (row A) of the contoured vane, a more uniform *BR* distribution takes place across the passage with respect to the planar one and for all the injection conditions; this allows the coolant flow to be more uniformly distributed among the holes. Then it can be deduced that at low blowing conditions, i.e., at $MFR=0.5\%$ and partially also at $MFR=0.75\%$ (not shown), main flow ingestion takes place all over the holes as *BR* values are zero. Finally these data confirm that the pressure gradient across the passage is smaller.

Very similar distributions characterize the following rows of the two considered endwall geometries. Only the last injection row (row D) in the contoured endwall shows slightly reduced *BR* values for the highest injection conditions. Finally, ingestion of the main flow partially takes place also along row B at the lowest $MFR=0.5\%$.

3.3 Cooled Endwall. Figure 13 and 14 show the energy loss coefficient distributions for four selected blowing conditions, which corresponds to $MFR=0.5$, 1.0, 2.0, and 2.5%, respectively, and the two tested endwall geometries, i.e., planar and contoured. Each plot shows one single pitch flow. In the contoured case it includes the wake of the profile between the two cooled passages. In the planar case, only the suction side passage endwall is cooled. Data obtained for the planar endwall are only reported for comparison purposes. The reader can refer to Ref. [13] for a deeper discussion of these data.

In the planar case (Fig. 13), low momentum coolant injection enforces the passage vortex with respect to the uncooled case. The loss core related to the passage vortex becomes much wider and the peak growths up to more than 35%. Increasing the *MFR*, the secondary loss coefficient initially comes back to an uncooledlike distribution, with only an increase in the losses associated to the corner vortex. Then the passage vortex related loss core moves closer to the endwall and reduces in intensity, while the corner vortex remains unchanged. Finally, when injecting at large mass flow ratio, the high energy fluid introduced at the endwall along the flow channel is captured by the passage vortex and acts on the

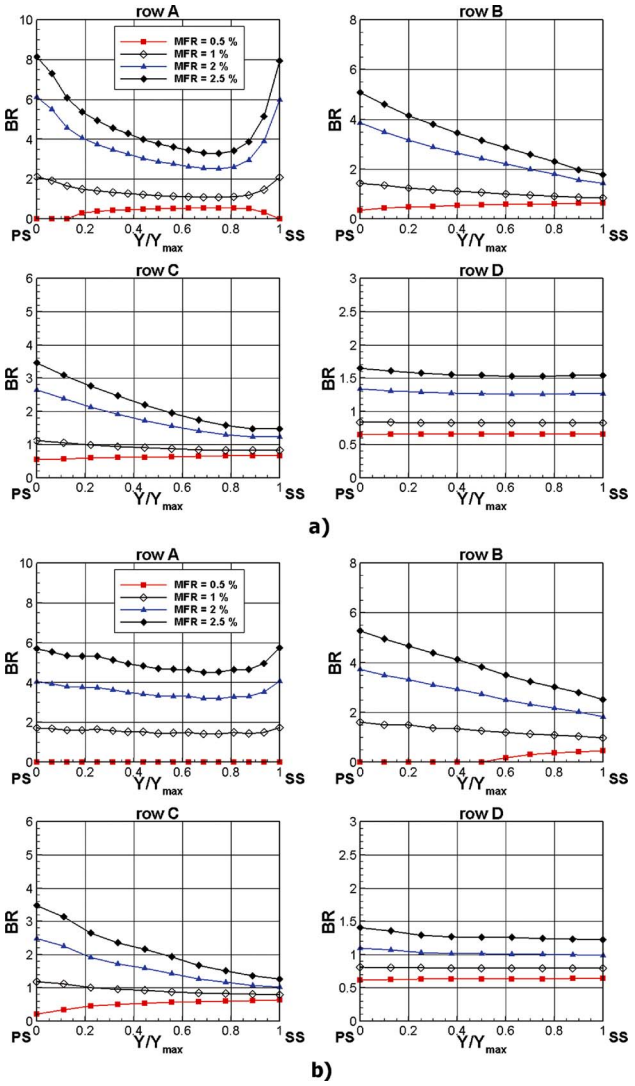

Fig. 12 Local blowing ratios: (*a*) planar and (*b*) contoured cascades

vortex itself by increasing the streamwise velocity and so producing a stretching of the vortex structure. This results in an almost two-dimensional wake structure.

Moving to the contoured case, as a general comment, one can observe that increasing the coolant mass flow rate produces secondary flow modifications similar to those already observed in the planar case. However these modifications appear to be of minor impact. When coolant is injected at low mass flow ($MFR=0.5\%$) (Fig. 14(*a*)), a partial flow ingestion takes place in the first two hole rows, so contributing to increase losses. Moreover, the coolant is injected with low momentum and remains inside of the thick endwall boundary layer; so this low energy fluid is going to enforce the loss core related to the passage vortex. In fact, the loss core related to the passage vortex widens pitchwise and the peak loss grows from 32% up to about 40% with respect to the uncooled/solid case.

A similar behavior also stands for the case at $MFR=1.0\%$ (Fig. 14(*b*)). The larger coolant injection causes only a small enlargement of the loss core without any significant modification in the wake structure.

For a further increase in the injection rate, i.e., for $MFR=2.0\%$ (Fig. 14(*c*)), there is a unique high loss region extending over a large portion of the endwall, but it is squeezed against the wall. This spanwise reduction in the loss region is the result of the

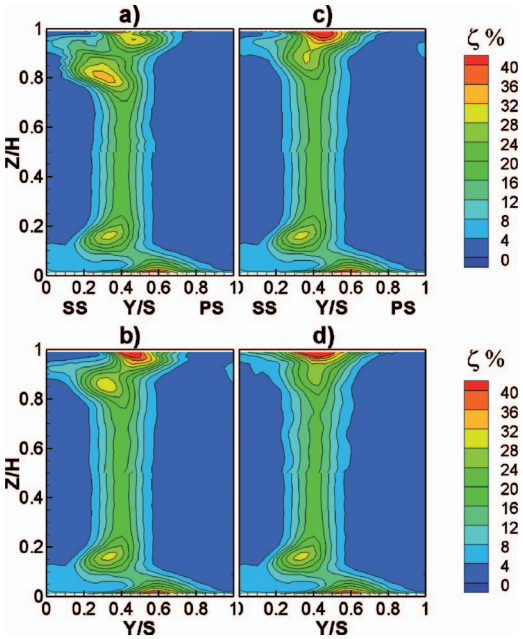

Fig. 13 Planar cascade secondary kinetic energy loss (primary) coefficient (X/c_{ax}=150%): (*a*) *MFR*=0.5%, (*b*) *MFR*=1.0%, (*c*) *MFR*=2.0%, and (*d*) *MFR*=2.5%

injected high momentum fluid, which somehow re-energizes the endwall boundary layer, counteracting the recompression occurring at the outer diameter, thus reducing its thickness.

Increasing the coolant to mainstream mass flow rate up to the maximum investigated value of 2.5% (Fig. 14(*d*)), the whole low energy layer is confined even closer to the endwall surface. The location of the loss core is displaced toward the wake suction side. This is a clear indication that the crossflow at the endwall produced by the secondary flows is strongly reduced; the reason is that the high momentum of the injected flow is going to counter-

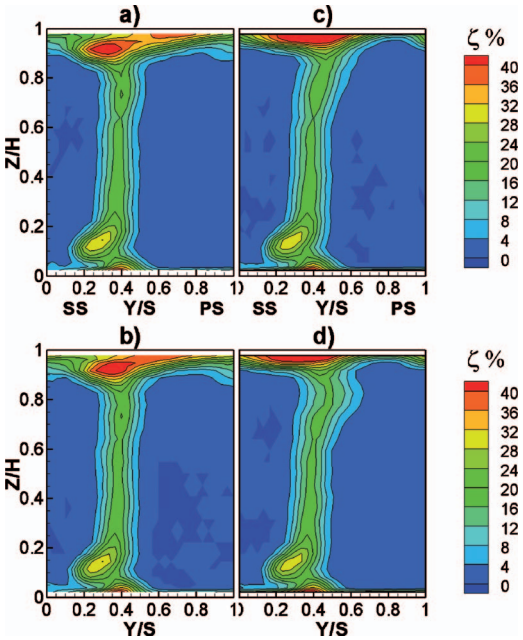

Fig. 14 Contoured cascade secondary kinetic energy loss (primary) coefficient (X/c_{ax}=150%): (*a*) *MFR*=0.5%, (*b*) *MFR*=1.0%, (*c*) *MFR*=2.0%, and (*d*) *MFR*=2.5%

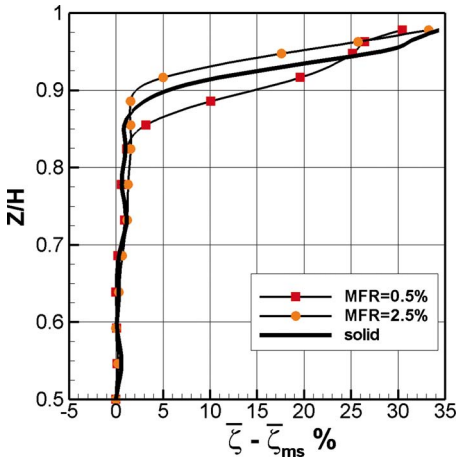

Fig. 15 Spanwise primary loss distribution

act the secondary flow action driving the passage vortex from the pressure to the suction side of the passage. Another interesting feature is the appearance of a twisted wake. This is certainly related to the combined effects of the reduced endwall crossflow and to the increased coolant jets momentum. But, from the present results, it was not possible to explain the reason why a tangential crossflow took place, which was able to move pitchwise the upper part of the wake.

Local flow field data were then mass averaged over the pitch to obtain the spanwise distributions of the loss coefficient and deviation angle. The results are shown in Figs. 15 and 16, respectively. Only the contoured outer diameter half span data are reported as no differences were found on the hub side. Moreover, to make the figures clearer, only data belonging to the minimum (*MFR*=0.5%) and maximum (*MFR*=2.5%) injection conditions are reported together with the solid distributions.

Coolant to mainstream mass flow ratio variation only marginally changes the spanwise loss coefficient distribution (Fig. 15). Differences are limited to the region extending up to 20% from the profiled endwall. At low injection rates (*MFR*=0.5% and 1.0%, even if not shown) a loss increase takes place with respect to the uncooled case, which corresponds to a thicker high loss region. Increasing the injection condition up to 2.0% and 2.5%, a similar peak value at the wall can be observed, but the loss distribution progressively reduces its spanwise extension. At larger injection rate of 2.5% the region affected by the secondary losses is reduced to about 10% of the span.

Looking at the deviation angle distributions for different injec-

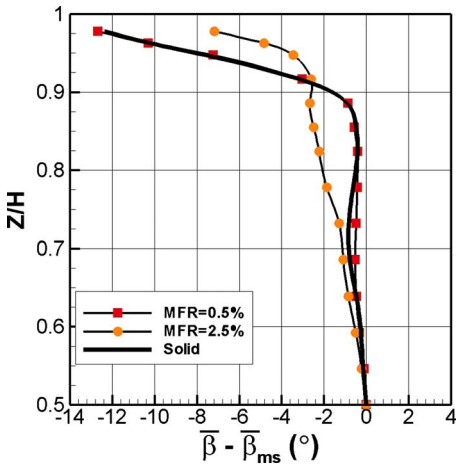

Fig. 16 Spanwise flow angle deviation distribution

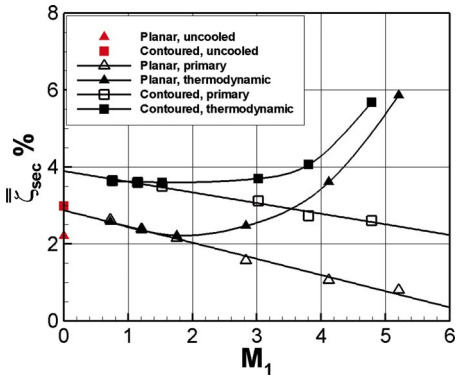

Fig. 17 Mass averaged primary and thermodynamic secondary energy loss coefficients versus M_1

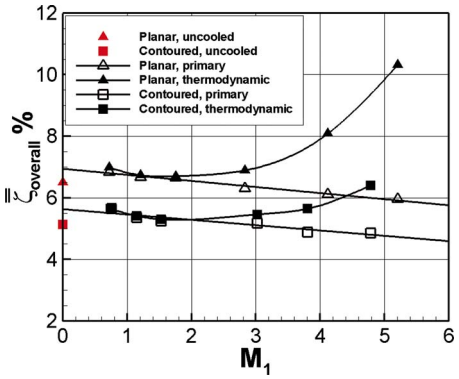

Fig. 18 Mass averaged primary and thermodynamic overall energy loss coefficients versus M_1

tion conditions (Fig. 16), the curves for the two lowest *MFR* (0.5% and also for 1.0%) practically overlap the uncooled one; no secondary deviation angle takes place up to 85% of the span, then there is a strong overturning growing up to about 13 deg at the contoured endwall. As previously said, this large deviation is mainly due to the axial velocity reduction taking place in the outer diameter region downstream of the vane exit. Relevant differences take place for the larger injection conditions. For $MFR=2.0\%$ the overturning angle at the endwall undergoes a general reduction (9 deg at the wall), while it increases while moving toward the midspan. For $MFR=2.5\%$, this behavior goes on with a further reduction at the wall (7 deg) and a further increase in the middle of the passage.

3.4 Mass Averaged Results. To quantify the effect of coolant injection on the cascade aerodynamic performance, overall energy losses have been estimated by mass averaging the flow data all over the vane passage. The so-called thermodynamic loss coefficient proposed by Kost and Holmes [20] was also computed as follows:

$$\bar{\bar{\zeta}}_{th} = \frac{m_\infty(\bar{\bar{U}}_{2is}^2 - \bar{\bar{U}}_2^2) + m_c(U_{2is,c}^2 - \bar{\bar{U}}_2^2)}{(m_\infty + m_c)\bar{U}_{2is,ms}^2} \tag{2}$$

This formulation takes into account the energy related to the injected flow; thus it also includes losses inside the cooling holes. Primary losses, on the contrary, do not take into account the coolant energy; so, when the injection flow is risen, primary losses are going to be decreased. The secondary loss is obtained by subtracting the pitchwise averaged loss at midspan from the total loss. Figure 17 shows the primary and thermodynamic secondary losses for the tested injection conditions and the two endwall configurations, i.e., planar and contoured. For the profiled endwall case, these secondary loss coefficients were computed by mass averaging over the contoured half span (50–100%). Figure 18 shows instead the overall losses, including the profile and flat and contoured side secondary losses. Solid endwall data are also presented for comparison. Data are plotted versus the inlet loss free blowing ratio parameter M_1 instead of the mass flow rate, as it is better related to local injection conditions.

Planar and contoured secondary losses (Fig. 17) show the same behavior versus injection conditions; the primary loss coefficients linearly decrease while a paraboliclike trend characterizes the thermodynamic ones. The contoured vane shows a larger loss of about 1% up to $M_1=3.0$; this difference reduces the increase in the injected coolant flow. This means that, regardless of higher loss level, even for the contoured vane, the beneficial effects of injection on secondary flow reduction are present.

Secondary thermodynamic losses remain almost constant for blowing ratios up to $M_1=3.0$; then for larger blowing rates a quite large loss increase takes place. So, as far as secondary losses are concerned, an optimum injection condition for the contoured case can be established at $M_1=1.5$. This optimum condition corresponds (Fig. 17) to an injected mass flow rate $MFR=1.0\%$. It can be observed that for the planar endwall the optimum blowing condition occurred at a higher blowing rate of about $M_1=2.0$, which in anyway corresponds to the same coolant flow rate $MFR=1.0\%$.

Figure 18 shows the overall losses for the two endwall configurations versus the blowing rate. It has to be noted that the contoured cascade, regardless of higher secondary losses on the contoured side, performs better than the planar one, both from the primary and thermodynamic point of views, for all the injection conditions. This is due to the significant reduction in both profile and planar side secondary losses induced by contouring; these improvements largely balance the larger profiled side secondary loss.

Even for overall losses it can be identified as a minimum loss for both endwall geometries; such a condition takes place almost at the same blowing ratio indicated in Fig. 17 for secondary losses, i.e., at about $M_1=1.5$ for the contoured vane and at $M_1=2.0$ for the planar vane.

4 Conclusions

The experimental investigation on the combined effects of endwall contouring and coolant injection has led to the following conclusions.

- Endwall contouring produces an overall loss reduction of about 20% with respect to the planar cascade. Most of this reduction is related to a smaller profile loss as total secondary losses undergo a quite limited increase; on the flat side there is a loss decrease, while on the contoured side a growth of about the same amount takes place.
- The pressure distribution on the contoured endwall showed a reduced aerodynamic loading in the front part of the passage; this provided a more uniform local blowing ratio distribution in the first row of holes located upstream of the vane leading edge.
- Coolant injection induces a reduction in the intensity of secondary flows, i.e., as for the planar vane, but secondary losses on the contoured side are always larger than those on the planar vane. Conversely, global losses of the contoured geometry are always lower, whatever injection rate is concerned.
- A unique minimum loss injection condition was found for both tested geometries, which corresponds to an injected mass flow rate of about 1.0%.

The present investigation on the aerodynamic aspects is the starting point for a more extended analysis on the thermal performance of a contoured film cooled endwall that will be carried out in the future.

Acknowledgment

The authors wish to thank Professor C. Rizzi and Dr. D. Regazzoni for the rapid prototyping and Mr. V. Biondi and E. Gatti for the appreciated technical support.

Nomenclature

BR = local blowing rate $(\rho_c U_c)/(\rho_\infty U_\infty)$
c = blade chord
C_d = discharge coefficient
D = hole diameter
H = blade height
H_{12} = shape factor δ^*/θ
L = hole length
M_1 = inlet blowing ratio $\sqrt{(p_{t,c}-p_1)/(p_{t,1}-p_1)}$
m = mass flow rate
Ma = Mach number
MFR = overall coolant to mainstream mass flow ratio m_c/m_∞
P = hole pitch
$\mathrm{Re}_{2\mathrm{is}}$ = isentropic outlet Reynolds number $U_{2\mathrm{is}}c/\nu$
s = blade pitch
Tu = turbulence intensity $\sqrt{0.5(\overline{u'^2}+\overline{v'^2})}/U_1$ (%)
U = local mean velocity $\sqrt{u^2+v^2+w^2}$
u,v,w = streamwise, transverse, and spanwise velocity components
X,Y,Z = cascade coordinate system
α = injection angle
β = flow angle (axial direction)
δ = boundary layer thickness
δ^* = displacement thickness
ν = kinetic viscosity
θ = momentum thickness
ρ = flow density
ζ = local energy loss coefficient $(U_{2\mathrm{is}}^2-U_2^2)/\bar{U}_{2\mathrm{is,ms}}^2$
Ω = nondimensional vorticity $\Omega_s c/U_1$

Subscripts

1 = inlet
2 = exit
c = cooling flow
is = isentropic condition
ms = at midspan
pr = primary
s = streamwise
th = thermodynamic
∞ = freestream

Overbar

$\bar{}$ = time averaged, pitch averaged
$\tilde{}$ = mass averaged
$'$ = rms

References

[1] Dejc, E., Filipov, G. A., and Lazarev, L. Ya., 1965, *Atlas of Axial Turbine Blade Characteristics*, Machinostroenie, Moscow.
[2] Boletis, E., 1985, "Effects of Outer Diameter Endwall Contouring on the Three-Dimensional Flow Field in an Annular Turbine Nozzle Guide Vane: Part I—Experimental Investigation," ASME J. Eng. Gas Turbines Power, **107**, pp. 983–990.
[3] Moustapha, S. H., and Williamson, R. G., 1986, "Effect of Two Endwall Contours on the Performance of an Annular Nozzle Cascade," AIAA J., **24**(9), pp. 1524–1530.
[4] Dossena, V., Perdichizzi, A., and Savini, M., 1999, "The Influence of Endwall Contouring on the Performance of a Turbine Nozzle Guide Vane," ASME J. Turbomach., **121**, pp. 200–208.
[5] Sieverding, C. H., and Wilputte, Ph., 1981, "Influence of Mach Number and End Wall Cooling on Secondary Flows in a Straight Nozzle Cascade," ASME J. Eng. Power, **103**, pp. 257–264.
[6] Jabbari, M. J., Marston, K. C., Eckert, E. R. G., and Goldstein, R. J., 1996, "Film Cooling of the Gas Turbine Endwall by Discrete-Hole Injection," ASME J. Turbomach., **118**, pp. 278–284.
[7] Zhang, L. J., Jaiswal, R. S., 2001, "Turbine Nozzle Endwall Film Cooling Study Using Pressure Sensitive Paint," ASME Paper No. 2001-GT-0147.
[8] Friedrichs, S., Hodson, H. P., and Dawes, W. N., 1996, "Distribution of Film-Cooling Effectiveness on a Turbine Endwall Measured With the Ammonia and Diazo Technique," ASME J. Turbomach., **118**, pp. 613–621.
[9] Friedrichs, S., Hodson, H. P., and Dawes, W. N., 1997, "Aerodynamic Aspects of Endwall Film-Cooling," ASME J. Turbomach., **119**, pp. 786–793.
[10] Kost, F., Nicklas, M., 2001, "Film-Cooled Turbine Endwall in a Transonic Flow Field: Part I—Aero-Dynamic Measurements," ASME Paper No. 2001-GT-0145.
[11] Nicklas, M., 2001, "Film-Cooled Turbine Endwall in a Transonic Flow Field: Part II—Heat Transfer and Film-Cooling Effectiveness," ASME Paper No. 2001-GT-0146.
[12] Knost, D. G., Thole, K. A., 2004, "Adiabatic Effectiveness Measurements of Endwall Film-Cooling for a First Stage Vane," ASME Paper No. GT-2004-53326.
[13] Barigozzi, G., Benzoni, G., Franchini, G., and Perdichizzi, A., 2005, "Aerodynamic Measurement Over a Film Cooled Nozzle Vane Endwall," *Proceedings of the Sixth European Conference on Turbomachinery Fluid Dynamics and Thermodynamics*, G. Bois, C. Sieverding, M. Manna, and T. Arts, eds., Vol. 2, pp. 791–801.
[14] Barigozzi, G., Benzoni, G., Franchini, G., and Perdichizzi, A., 2006, "Fan-Shaped Hole Effects on the Aero-Thermal Performance of a Film Cooled Endwall," ASME J. Turbomach., **128**, pp. 43–52.
[15] Burd, S. W. and Simon, T. W., 2000, "Effects of Slot Bleed Injection Over a Contoured Endwall on Nozzle Guide Vane Cooling Performance: Part I—Flow Field Measurements," ASME Paper No. 2000-GT-199.
[16] Oke, R. A., Simon, T. W., Burd, S. W., Vahlberg, R., 2000, "Measurements in a Turbine Cascade Over a Contoured Endwall: Discrete Hole Injection of Bleed Flow," ASME Paper No. 2000-GT-214.
[17] Gustafson, R., Mahmood, G. I. and Acharya, S., 2007, "Flowfield in a Film-Cooled Three-Dimensional Contoured Endwall Passage: Aerodynamic Measurements," ASME Paper No. GT2007-28154.
[18] Barigozzi, G., Franchini, G., and Perdichizzi, A., 2007, "Inlet Turbulence Intensity Effect on Endwall Film Cooling," *Proceedings of the Seventh European Conference on Turbomachinery Fluid Dynamics and Thermodynamics*, K. D. Papailiou, F. Martelli, and M. Manna, eds., pp. 1105–1116.
[19] Gregory-Smith, D. G., Graves, C. P., and Walsh, J. A., 1988, "Growth of Secondary Losses and Vorticity in an Axial Turbine Cascade," ASME J. Turbomach., **110**, pp. 1–8.
[20] Kost, F. H., and Holmes, A. T., 1985, "Aerodynamic Effect of Coolant Ejection in the Rear Part of Transonic Rotor Blades," AGARD CP 390 Heat Transfer and Cooling in Gas Turbines, Bergen, Norway.